A P-Matrix Based Model for SAW Grating Waveguides Taking into Account Modes Conversion at the Reflection

Marc Solal, *Member, IEEE*, Vincent Laude, *Member, IEEE*, and Sylvain Ballandras

***Abstract*—Several models exist for analyzing the waveguiding effect of a reflective grating. On the one hand, there are models based on scalar waveguide theory. These models consider that a device can be described as being made of several regions having different velocities. On the other hand, an extension of the coupling of modes (COM) model taking into account the transverse dimension has been developed. This paraxial COM model predicts that guidance is possible even when there is no velocity difference between the interior and the exterior of the grating region. Guidance, under such circumstances, is due only to differences in reflectivity between regions. Following from this insight, a new approach has been developed: guided modes and the continuum of radiating modes are first determined. At each period, reflections then are considered as occurring only in the reflective regions, so that the modes are truncated. Thus, at each reflection (and transmission), each mode is converted into a distribution of all modes. Dispersion curves very similar to those shown by other researchers are obtained by this method. They show, in particular, the existence of guided modes even when the wave velocity in all regions is identical. This model can be used to more easily analyze practical devices and exhibits a good agreement with experimental results.**

I. Introduction

Several models exist for analyzing the wave-guiding effect of a reflective grating. Some authors use models based on standard scalar theory [1]–[4]. These models consider that a device can be described as being made from several layers having different velocities. A general procedure, using a stack matrix, allows one to derive the dispersion equation and the mode shapes for an arbitrary number of layers. All the layers are considered homogeneous, i.e., the reflectivity is neglected in the derivation of modes.

Other models, which have used both reflectivity and velocity differences to determine dispersion curves, have been published. The paraxial coupling of modes model developed originally by Haus [5] allows for the possibility that there exist guidance due exclusively to differences in reflectivity between adjacent regions. This approach has been followed by Hirota and Nakamura [6]. Hartmann *et al.* [7] were able to derive the dispersion curve for grating waveguides accounting for reflection.

Another approach was initiated by Rooth [8]. The idea presented is to decompose each period in the transverse direction into several unit cells. This leads to the definition of 2D-P matrices recently presented [9].

In [10] and [11], a method based on the P-matrix model is presented. In this approach, the reflectivity is introduced at the modes determination stage by choosing for the reflective regions a velocity such that the grating period is equal to half a wavelength for the lower edge frequency of the stop band. In order to obtain correct results, especially in the case of weak guiding conditions, the guided modes are not sufficient, and a continuum of radiating waves has to be taken into account. A P-matrix-based model taking into account guided modes and the continuum was developed. This model allowed us to describe successfully spurii at high frequencies for transversely coupled filters (TCF). However, several configurations cannot be analyzed with this model. In particular, for doubly rotated quartz devices [12], [13], the directivity is such that a mode exists at both edges of the stop band. Higher Q and transverse modes have been experimentally observed for the lower edge resonance, but only one resonance with lower Q is present for the higher edge resonance. It is our interperetation that the lower frequency resonance is guided but the higher is not.

The drawbacks of our previous model are, first, that the reflection coefficient used for the P-matrix is a two-dimensional (2-D) reflection coefficient that assumes an infinite aperture. Second, that the mode shapes are assumed unchanged after reflection. Modes have been suggested to be reflected only in reflective regions, implying that the amount of truncation of reflected modes is not negligible [4]. However, our previous trials using this assumption were not successful. Our understanding is that the reflectivity difference already was included in the model by the velocity choice, and that it did not need to be included twice.

This paper develops a different approach that is still based on the P-matrix model. The mode and continuum determination is done without correcting for the reflectivity effect in the velocities. In other words, for reflective regions, the velocity is chosen so that the grating period is equal to half a wavelength for the Bragg frequency, i.e., at the center of the stop band. This results in mode frequencies that do not correlate with experimental results.

Manuscript received November 12, 2003; accepted August 3, 2004.

M. Solal is with Temex, BP 232, F-06904, Sophia Antipolis Cedex, France (e-mail: marc.solal@temex.fr).

V. Laude and S. Ballandras are with the LPMO département, Institut FEMTO-ST, Centre National de la Recherche Scientifique UMR 6174, F-25044 Besançon Cedex, France.

In particular, even the number of guided modes very often is incorrect.

We use this assumption for the determination of modes and continuum samples. The difference is now we consider that at each period reflection is occurring only in the reflective regions so modes become truncated at each reflection. Conversely, transmission is considered to be 1 for a region with no reflectivity. Thus, at each reflection (or transmission), each mode is converted into a distribution of all modes. This approach was implemented and compared successfully to Haus' results [5] in the case of isotropic material as well as to experimental results for resonators on a doubly rotated quartz cut.

II. Dispersion Curve and Eigen Modes

A. Determination of Modes and Continuum Samples

The first step in the model is to determine guided modes and continuum samples. We use a procedure already described in detail in [11]. We only recall here the basic principles.

We consider a symmetric structure comprising $2N+1$ layers. In this first step, all layers are assumed to be homogeneous. The slowness curves for all materials are known, including the imaginary branches [14]–[16]. The classical parabolic approximation may be used as well as numerical results from these more sophisticated methods. The basic assumptions [1] are that the surface wave is accurately described by a scalar function, and that the wave polarizations are similar in all regions. Under these assumptions, it is possible to apply a standard theory:

- The wave vector component k_x along the propagation direction is identical for all layers.
- In each internal layer, indexed i, the transverse wave vector component k_y is known from k_x through the slowness curve of the layer, and two opposite determinations of k_y are possible for symmetric cuts. Then in layer i, the mode amplitude has the form:

$$g_i(y) = A_i \cos(k_{y,i} y) + B_i \sin(k_{y,i} y). \tag{1}$$

For the external medium, depending on k_x, the transverse component of the wave vector can be imaginary or real. In the first case, only the determination corresponding to an exponential decrease is kept, and the mode amplitude is:

$$\begin{aligned} g_{N+1}(y) &= c \exp(-b\,|y - y_N|), \\ b &= |\mathrm{Im}(k_{y,N+1})|, \end{aligned} \tag{2}$$

while in the second case both determinations can be kept:

$$\begin{aligned} g_{N+1}(y) = c.\exp(-jk_{y,N+1}(y - y_N)) \\ + d.\exp(jk_{y,N+1}(y - y_N)). \end{aligned} \tag{3}$$

Keeping both of the two possible opposite determinations of $k_{y,N+1}$ in (3) corresponds to considering plane waves propagating in both the $+y$ and the $-y$ directions for a given k_x. This is strictly similar to the standard angular spectrum of waves theory for diffraction [17] in which both negative and positive $k_{y,N+1}$ are considered.

The boundary conditions are applied at the interfaces between two layers. Under our assumptions, $g(y)$ and its first derivative along y are continuous. Then, depending on the evanescent or propagative nature of k_y in the external material, the solutions are a set of discrete guided modes or a continuum of waves. By using a general stack matrix procedure, one can deal with geometries involving an arbitrary number of layers.

B. Derivation of the Dispersion Curve

In the following, the amplitude of modes is denoted $g_n(y)$. We assume that the mode amplitudes are orthogonal, i.e.:

$$\int_{-\infty}^{\infty} g_k(y) g_1^*(y) dy = 0 \text{ if } k \text{ and l are different.} \tag{4}$$

The same relation is assumed between two continuum samples as well as between a continuum sample and a mode. The discrete modes are normalized in order to have a unit norm. The continuum is sampled with an increment Δky, and the samples are normalized to have a norm equal to $\sqrt{\Delta ky}$. With this normalization, discrete modes and continuum samples are processed exactly in the same way. In the subsequent presentation, the term mode is used for both guided modes and continuum samples.

Any wave amplitude $f(y)$ can be projected to the mode base through:

$$\begin{aligned} f(y) &\cong \sum_i f_i . g_i(y), \\ f_i &= \int f(y) g_i^*(y) . dy. \end{aligned} \tag{5}$$

The mode orthogonality assumption was verified by numerically checking the convergence of (5).

We examine here the scattering matrix for one grating period. This matrix relates outgoing wave amplitudes at the left and the right period boundaries sg and sd (defined at the center of spaces between two consecutive electrodes) to the left and right incoming waves amplitudes eg and ed.

$$\begin{bmatrix} \begin{bmatrix} sg_1 \\ \cdot \\ sg_N \end{bmatrix} \\ \begin{bmatrix} sd_1 \\ \cdot \\ sd_N \end{bmatrix} \end{bmatrix} = \begin{bmatrix} \begin{bmatrix} S11 \\ \\ \\ S21 \end{bmatrix} & \begin{bmatrix} S12 \\ \\ \\ S22 \end{bmatrix} \end{bmatrix} \cdot \begin{bmatrix} \begin{bmatrix} eg_1 \\ \cdot \\ eg_N \end{bmatrix} \\ \begin{bmatrix} ed_1 \\ \cdot \\ ed_N \end{bmatrix} \end{bmatrix}. \tag{6}$$

For a symmetric period, the right and left sides are equivalent so that $S22 = S11$ and $S21 = S12$ by reciprocity. Directive cuts can be modeled simply by adding a phase term to $S11$ and the opposite phase term to $S22$.

If we consider the i-th mode entering one period, this mode propagates half a period before it is reflected or transmitted. Then, the reflected wave amplitude at the center of the electrode is:

$$\begin{aligned} \text{rect}(y).g_i(y) &= \sum_i P_{i,j} g_j(y), \\ P_{i,j} &= \int \text{rect}(y).g_i(y).g_j^*(y).dy, \end{aligned} \tag{7}$$

where rect(y) is a function defined to be equal to unity in the reflective regions and to zero in the nonreflective regions. Assuming that reflection results in a grating of the mode shapes, the reflection and transmission matrices are given by:

$$\begin{aligned} S11_{i,j} &= -j.r.P_{j,i}.\exp\left(-j.\frac{\varphi_i+\varphi_j}{2}\right) = S22_{i,j}, \\ S12_{i,j} &= \left((t-1)+\delta_{i,j}\right).P_{j,i}.\exp\left(-j.\frac{\varphi_i+\varphi_j}{2}\right) \\ &= S21_{i,j}, \end{aligned} \tag{8}$$

where r and t are the reflection and transmission coefficients for one electrode, φ_i is the phase of the i-th mode for one period, and $\delta_{i,j}$ is the Kronecker symbol.

From (6), it is straightforward to derive the transfer matrix relating waves propagating in the right and left directions at the left boundary to the waves propagating in the left and right directions at the right boundary:

$$\begin{bmatrix}[sg]\\[eg]\end{bmatrix} = \begin{bmatrix}T11\ T12\\T21\ T22\end{bmatrix}\begin{bmatrix}[ed]\\[sd]\end{bmatrix}, \tag{9}$$

$$\begin{aligned} T11 &= \left(-S11.S12^{-1}S22 + S12\right), \\ T12 &= S11.S12^{-1}, \\ T21 &= -S12^{-1}S22, \\ T22 &= S12^{-1}. \end{aligned} \tag{10}$$

By computing the eigenvalues for different frequencies of the transfer matrix, it is possible to plot the dispersion curve obtained with this model. The eigenvectors of the matrix T give the eigenmodes of the structure (i.e., the transverse amplitudes of the waves in the two directions) that propagate without deformation. These eigenmodes are found as linear expansions on transverse modes and continuum samples. Note that the eigenmodes of the structure resemble those of the paraxial coupling of modes (COM) model—an amplitude shape for both the wave propagating to the right and left directions. In general these two amplitudes are different; however, they are identical in the stop band.

C. Results for a Simple Isotropic Case

For validation, we start to consider the very simple case examined by Haus [5]. One reflective layer of width $2W$ is placed in an infinite nonreflective medium. The two materials are considered isotropic. The reflection coefficient is assumed to be proportional to the frequency. For each frequency, the number of eigenvalues is $2N$ where N is the total number of modes and continuum samples. When visualizing the dispersion curve, it is difficult to distinguish between all these values, but it is easy to visualize the different stop bands, corresponding to eigenvalues with a modulus that is not equal to 1. Fig. 1 shows the results obtained for a grating of aperture $2W = 4.86\ \lambda_0$, $r = .079365$, having the same velocity in both inside and outside regions. The eigenvalues are considered to be of the form $\exp(-j\phi)$, so that the stop bands correspond to imaginary values of ϕ. The dispersion curve is very similar to the dispersion curve given in Fig. 1 in [5].

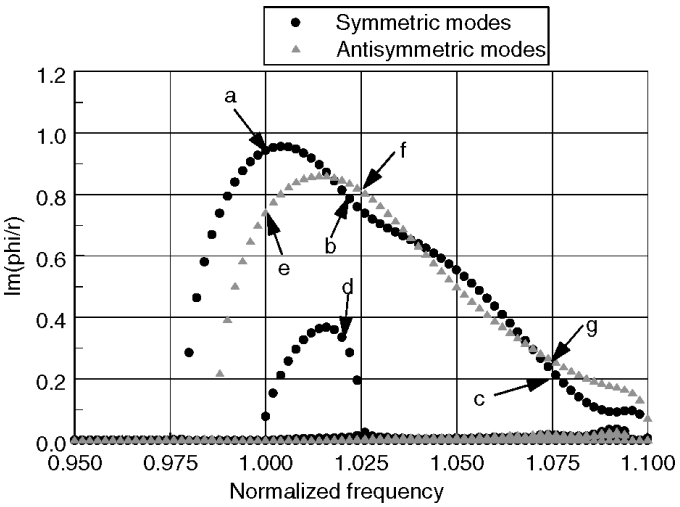

Fig. 1. Dispersion curves for the simple isotropic case. No velocity difference, grating aperture = 4.86 wavelengths, reflection coefficient = 0.079365 per period. The frequency is normalized to the Bragg frequency. Letters refer to the mode shapes plotted in Figs. 2 and 3.

In this case, because there is no velocity shift, no guided modes exist, and our model uses only the continuum samples. Figs. 2 and 3 show plots of different eigenmodes, showing a decreasing behavior outside the grating. Inside the stop band, the amplitude of propagating waves is the same in both directions. The shapes found here also are similar to the shapes found by Haus. A good fit also was obtained for other configurations published by Haus. These results validate the chosen model.

III. Devices Simulation

A. Device Simulation

In [11], we described in detail our P-matrix-based model for the analysis of waveguide devices. The principle is to derive the P-matrix for a single period, taking into account modes and continuum samples. This P-matrix model is generalized in the sense that the number of acoustical ports is no longer just two as is usually the case (left and right acoustical port), but two times the number NM of modes and continuum samples. Obviously, the number of

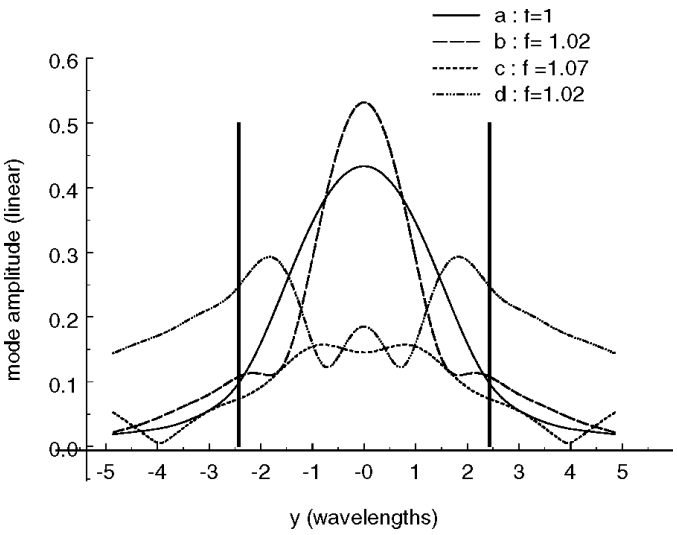

Fig. 2. Shapes of the symmetrical eigenmodes for the case of Fig. 1. Letters refer to Fig. 1. Vertical lines are the limits of the grating.

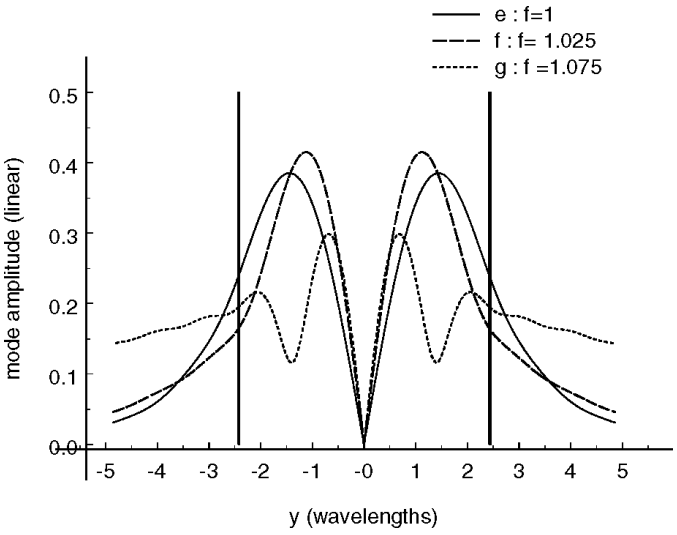

Fig. 3. Shapes of the antisymmetrical eigenmodes for the case of Fig. 1. The frequency is normalized to the Bragg frequency. Letters refer to Fig. 1. Vertical lines are the limits of the grating.

electrical ports may be different from 1 or 2. The P-matrix relates the currents I in the NE electrical ports and the NM output waves amplitudes at the left boundary sg and at the right boundary sd to the voltage V and the input wave amplitudes at the left and right boundaries eg and ed.

$$\begin{bmatrix} [I_{i=1,NE}] \\ [sg_{i=1,NM}] \\ [sd_{i=1,NM}] \end{bmatrix} = \begin{bmatrix} [M11] & [M12] & [M13] \\ [M21] & [S11] & [S12] \\ [M31] & [S21] & [S22] \end{bmatrix} \cdot \begin{bmatrix} [V_{i=1,NE}] \\ [eg_{i=1,NM}] \\ [ed_{i=1,NM}] \end{bmatrix}. \quad (11)$$

The scattering matrix is derived above, and the admittance matrix and the electroacoustic and acoustoelectric matrices are derived in [11].

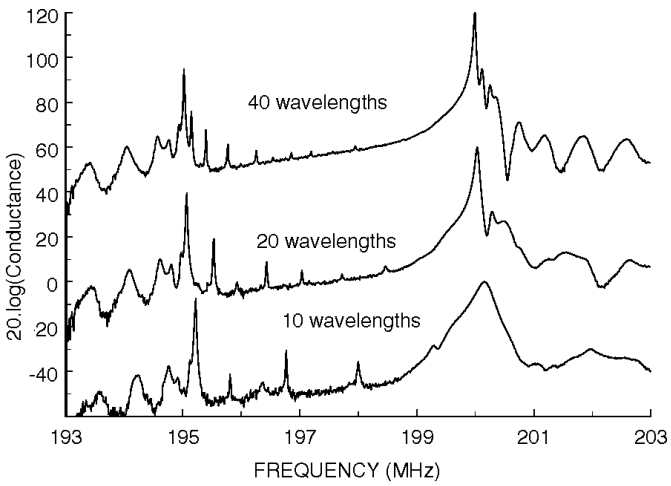

Fig. 4. Measured conductances for the long devices on doubly rotated quartz. The curves are shifted artificially.

The second step is to compute the P-matrix of the complete device by cascading the P-matrices of the unit cells. This operation needs several CPU hours because it involves large matrices (typically, we use 100 continuum samples). But there are methods to reduce this time for a periodic device either by optimizing the stacking by taking advantage of the repetition of identical sequences or by working in the eigenmodes basis.

It also is possible to derive the harmonic admittance $Y(\gamma)$ of a periodic structure from the P-matrix of a single period. The principle is to consider that the waves amplitudes at the right boundary are equal to the wave amplitudes at the left boundary multiplied by a phase term $\exp(-j2\pi\gamma)$. Then, it is straightforward to eliminate waves amplitudes from (11) and to derive $Y(\gamma)$. In particular, $Y(1/2)$ is the admittance of an infinite periodic transducer excited by an alternate potential figure $+V/-V$.

B. Results

We used our model to analyze synchronous resonators made on $(YXwlt)/-20°/-35°/+20°$ quartz. This quartz cut has a very large reflection coefficient compared to ST quartz while keeping a parabolic temperature dependence [12], [13]. It also has the property to be directive in the sense that the phase between reflection and transduction is 160° (under our notations, this phase is 0° for ST quartz and 180° for low metal thickness on 128° lithium niobate ($LiNBO_3$)). Then, a synchronous resonator made on this cut exhibits two resonances (neglecting the transverse modes). The main resonance is at the upper edge of the stop band, and the second resonance is at the lower edge of the stop band. Fig. 4 shows the measured conductances for long devices on this cut at 200 MHz. The metal thickness is 3800 Å, the period is 8.671 μm, the mark-to-pitch ratio is 0.6. The devices are synchronous resonators comprising a 200 wavelength transducer and two 10 wavelength gratings. Devices with acoustic apertures of 10, 20, and 40 λ were built. It is clearly seen on Fig. 4 that the Q

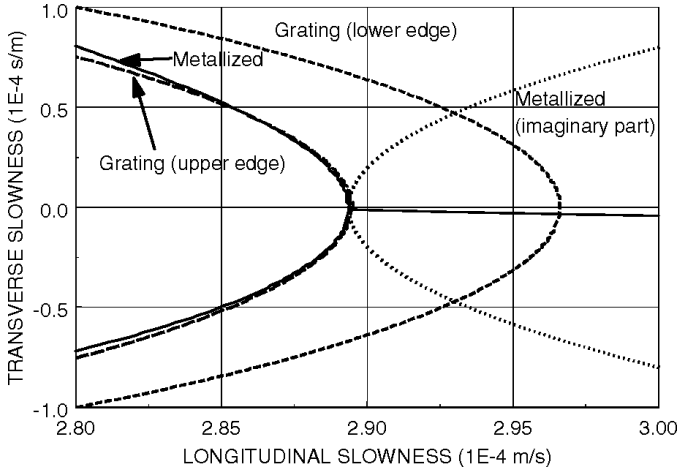

Fig. 5. Computed slowness curves for the doubly rotated quartz cut. The slowness curves are shown in busbars and in the grating for both the lower and upper edge of the stop band.

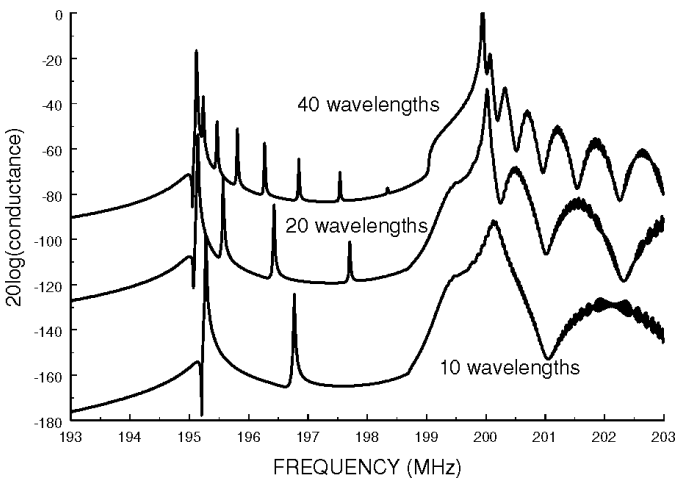

Fig. 6. Simulated harmonic conductances. The curves are shifted artificially, Re$[Y(1/2)]$ is plotted.

of the lower resonance is better than the Q of the higher frequency resonance, which is degraded when the aperture decreases. For the lower frequency, transverse modes are obtained, but the Q remains correct when the aperture decreases. Fig. 5 shows the computed slowness curves for our experiments. The slowness curve in the grating is computed using oblique wave finite element method/boundary element method (FEM/BEM) [15]. In the busbars regions, the real branches as well as the imaginary branches are computed [16]. The P-matrix parameters (reflection, velocity, etc.) are computed using the 2-D periodic FEM-BEM [18], [19]. For the grating region, Fig. 5 shows the slowness curves for the lower and for the upper edges of the stopband. It is clearly seen on Fig. 5 that the slowness curve for the upper edge is very close (and a little smaller) than the slowness curve for the busbars. This results in diffraction losses for the upper frequency resonance.

We used our model to compute the harmonic admittances $Y(1/2)$ for these three geometries. The slownesses used are the slownesses shown in Fig. 5. The parabolic approximation was used, and the power flow angle was neglected, although it is possible to include it as well as real slowness curves in our model. Absolutely no fitting parameter is used.

Fig. 6 shows the computed harmonic conductances. A good fit is obtained between the measured and computed data for the position of the modes as well as for the description of the Q degradation due to the aperture. The major difference between measurement and simulation is the existence of nonexpected modes in the measured data. It appears that these modes are antisymmetrical. For example, Fig. 7 shows the dispersion curve for antisymmetrical modes for the 10-wavelength device. The correspondence in frequency is very good. Similar results are obtained for the other apertures. The existence of these resonances is attributed to the non-null power flow angle.

Figs. 8–10 show the same comparison of the measured and simulated conductances for the same devices. The sim-

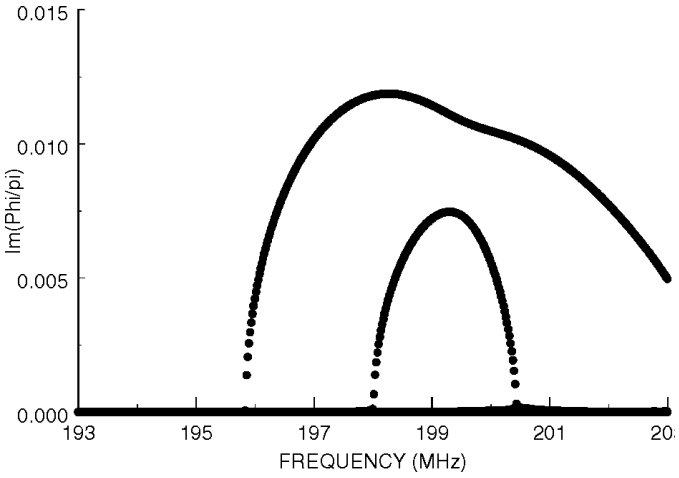

Fig. 7. Simulated dispersion curve for the antisymmetrical modes and a 10 λ aperture.

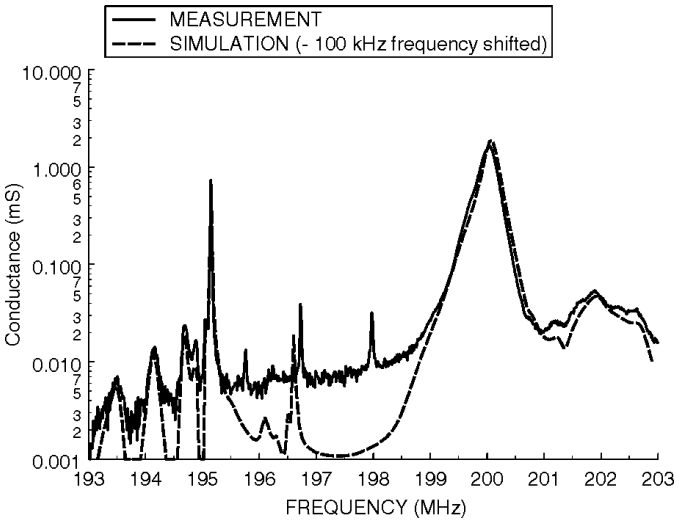

Fig. 8. Comparison between measured and simulated admittance for the 10 λ aperture device.

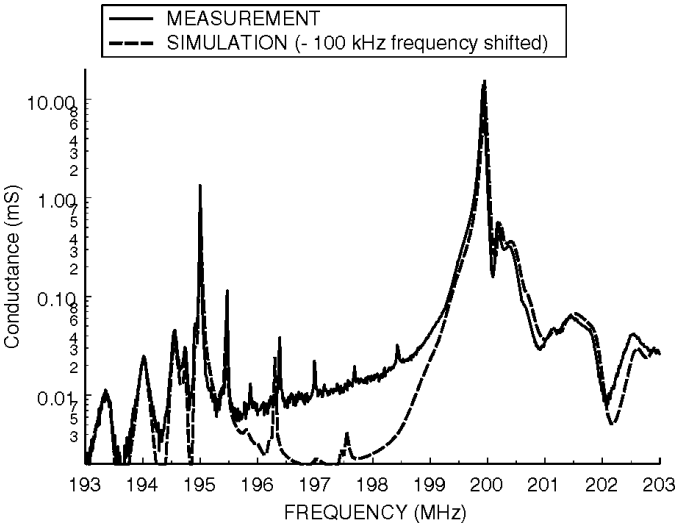

Fig. 9. Comparison between measured and simulated admittance for the 20 λ aperture device.

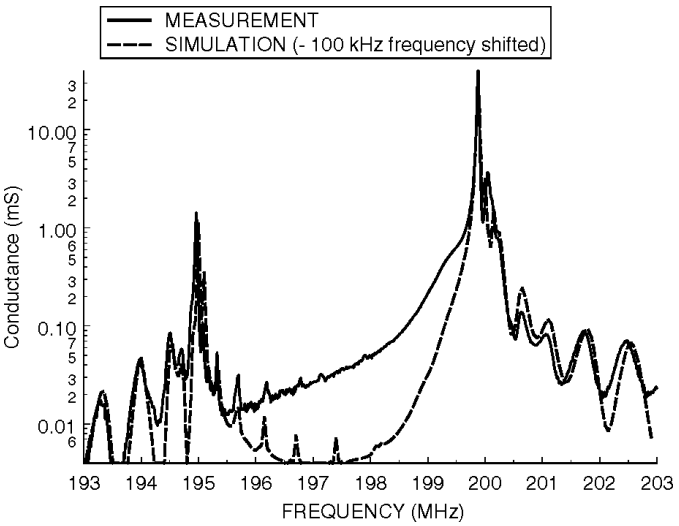

Fig. 10. Comparison between measured and simulated admittance for the 40 λ aperture device.

ulations were performed by cascading the P-matrices of the unit cells. The 100 continuum samples used for these simulations and the last continuum sample corresponds to a frequency in the range of 203 MHz. The results are plotted on a log scale to see a wide dynamic range. The fit is very good for the shape of the modes and their resonant frequencies. The difference for low levels of conductance (in the range of 0.01 to 0.1 mS) may be attributed to ohmic losses not taken into account in our model. This clearly demonstrates the validity of our model, which allows for the analysis of transverse modes as well as diffraction losses in reflective devices.

IV. Conclusions

A new P-matrix-based model has been developed for the analysis of surface acoustic wave (SAW) grating devices. This model accounts for the different reflectivities of the regions in the P-matrix as suggested in [4]. However, correct results were obtained only after choosing for the gratings the velocity corresponding the center of the stop band—which gives an incorrect number of modes—by including the continuum in the model and by using a fully populated scattering matrix accounting for all possible conversions at reflections. Then, results very similar to the paraxial COM were obtained for simple cases.

Our model allows one to predict both transverse modes as well as diffraction losses, which is not possible with standard scalar models. This model was used successfully for resonators on a directive cut of quartz. Slowness curves, and reflection coefficient were computed directly from material constants without any parameter fit.

Acknowledgments

The authors wish to thank W. Steichen for providing the measurement and D. Smalley for reviewing the manuscript.

References

[1] R. V. Schmidt and L. A. Coldren, "Thin film acoustic surface waveguide on anistropic media," *IEEE Trans. Sonics Ultrason.*, vol. 22, no. 2, pp. 115–122, Mar. 1975.

[2] D. P. Morgan, S. Richards, and A. Staples, "Development and analysis of analysis techniques for SAW transverse-coupled waveguide resonator filters," in *Proc. IEEE Ultrason. Symp.*, 1996, pp. 177–181.

[3] W. D. Hunt, T. Cameron, J. C. B. Saw, Y. Kim, and M. S. Suthers, "Modes profiles in waveguide-coupled resonators," in *Proc. IEEE Ultrason. Symp.*, 1992, pp. 45–50.

[4] G. Scholl, W. Ruile, and P. H. Russer, "P-Matrix modeling of transverse-mode coupled resonator filters," in *Proc. IEEE Ultrason. Symp.*, 1993, pp. 41–46.

[5] H. A. Haus, "Modes in SAW grating resonators," *J. Appl. Phys.*, vol. 48, pp. 4955–4961, Dec. 1977.

[6] K. Hirota and K. Nakamura, "Analysis of SAW grating waveguides using 2-D coupling-of-modes equations," in *Proc. IEEE Ultrason. Symp.*, 2001, pp. 115–120.

[7] C. S. Hartmann, V. P. Plessky, and S. Jen, "112° $LiTaO_3$ periodic waveguides," in *Proc. IEEE Ultrason. Symp.*, 1995, pp. 63–66.

[8] S. Rooth, "Narrowband surface acoustic wave filters with emphasis on long transducers," Ph.D. dissertation, Norvegian University of Science and Technology, Trondheim, Norway, July 1996.

[9] M. Mayer, G. Kovacs, A. Bergmann, and K. Wagner, "A powerful novel method for the simulation of waveguiding in SAW devices," in *Proc. IEEE Ultrason. Symp.*, 2003, pp. 720–723.

[10] M. Solal, "A mixed transverse modes and angular spectrum of waves model for the analysis of SAW transversely coupled resonator filters," in *Proc. IEEE Freq. Contr. Symp.*, 1999, pp. 945–949.

[11] ——, "A P-Matrix-based model for the analysis of SAW transversely coupled resonator filters including guided modes and a continuum of radiated waves," *IEEE Trans. Ultrason., Ferroelect., Freq. Contr.*, vol. 50, pp. 1729–1741, Dec. 2003.

[12] S. Ballandras, E. Briot, M. Solal, W. Steichen, M. Doisy, and J. M. Hodé, "A new triply rotated quartz cut for the fabrication

of low loss SAW filters," in *Proc. IEEE Ultrason. Symp.*, 2000, pp. 241–244.
[13] S. Ballandras, W. Steichen, E. Briot, M. Solal, M. Doisy, and J. M. Hodé, "A new triply rotated quartz cut for the fabrication of low loss IF SAW filters," *IEEE Trans. Ultrason., Ferroelect., Freq. Contr.*, vol. 51, pp. 121–126, Jan. 2004.
[14] K. Y. Hashimoto, "Analysis of SAWs obliquely propagating under metallic gratings," *Jpn. J. Appl. Phys.*, vol. 35, pp. 3006–3009, 1996.
[15] V. Laude and S. Ballandras, "Slowness curves and characteristics of surface acoustic waves propagating obliquely in periodic finite-thickness gratings," *J. Appl. Phys.*, vol. 4, pp. 1235–1242, 2003.
[16] M. Masson, V. Laude, and M. Solal, "Imaginary branches of SAW slowness curves," in *Proc. IEEE Ultrason. Symp.*, 2003, pp. 1704–1707.
[17] M. Kharusi and G. W. Farnell, "Diffraction and beam steering for surface-wave structures on anistropic substrates," *IEEE Trans. Sonics Ultrason.*, vol. SU-18, pp. 35–42, Jan. 1971.
[18] P. Ventura, J. M. Hodé, M. Solal, J. Desbois, and J. J. Ribbe, "Numerical methods for SAW propagation characterization," in *Proc. IEEE Ultrason. Symp.*, 1998, pp. 175–186.
[19] P. Ventura, J. M. Hodé, J. Desbois, and M. Solal, "Combined FEM and Green's function analysis of periodic SAW structure, application to the calculation of reflection and scattering parameters," *IEEE Trans. Ultrason., Ferroelect., Freq. Contr.*, vol. 48, pp. 1259–1274, Sep. 2001.

Marc Solal (M'95) was born in 1959. He received the engineer degree from Ecole Nationale Superieure de Physique de Marseille in 1981, a Docteur Ingénieur diploma in 1983, and the habilitation à diriger les recherches in 2000. Dr. Solal has been involved in the SAW field since 1981 as a member of the SAW research team of Thomson CSF and Thales. The Thales SAW activity was sold to Temex in 2002. His research efforts were first on SAW dispersive and bandpass transversal fillter design and analysis. Since 1991, his research interests have been on low loss filters for mobile radio, including device modeling, new piezoelectric material investigation, filter structure and design. Dr. Solal holds about 20 patents mainly in the SAW field. He is the director of the Laboratoire de Physique et de Microsonique, a joint laboratory between Temex and the Laboratoire de Physique et Métrologie des Oscillateurs of CNRS.

Vincent Laude (M'00) was born in Bourgla-Reine, France, in 1968. He received an Engineering Diploma in 1990 from the Ecole Supérieure d'Optique, and a Ph.D. in Physics in 1994 from Paris XI University, both in Orsay, France. He received his Habilitation à Diriger des Recherches from the Université de Franche-Comté in 2002.

From 1995 to 1999, he was a researcher at Thomson-CSF Corporate Research Laboratory (now Thales TRT) in Orsay, France, where he worked on various aspects of optical signal processing, wavefront sensing, and ultrashort laser pulses. In 2000, he joined Thomson-CSF Microsonics in Sophia-Antipolis, France, to work on surface acoustic wave propagation. At the end of the same year, he joined the Laboratoire de Physique et Métrologie des Oscillateurs, Centre National de la Recherche Scientifique, in Besançon, France. He is currently interested in the propagation of surface, interface, and guided acoustic waves, their interaction with microstructures, phononic band gap materials, and acousto-optics.

Vincent Laude is a member of IEEE/UFFC.

Sylvain Ballandras was born in 1965 in Strasbourg, France. He received the DEA in Acousto-Opto-Electronique et Vibrations and the Ph.D. degree in Science pour l'Ingénieur from the Université de Franche-Comté, Besançon, France.

He joined the Laboratoire de Physique et Métrologie des Oscillateurs (LPMO), Besançon, France, as a staff member in 1991. He has been working in the fields of SAW sensitivity to physical perturbations and in microtechnologies, such as LIGA and stereolithography. He received the Habilitation à Diriger des Recherches degree from the Université de Franche-Comté, in Besançon, France, in 1997. He joined Thomson Microsonics in Sophia Antipolis, France, for one year as a research engineer. He went back to the LPMO in 1998. Since 1999, he has been heading the Acoustics and Microsonics research group at the LPMO. His current interests are in the application of SAW devices (sensors) in the development of numerical models and new technologies for ultrasound transducers devoted to acoustic imaging and nondestructive control.